

Fine electronic structure and 5f-electron localized-itinerant transition in uranium films

Yun Zhang(张云), Jian Wu(吴健), Ying Jiang(蒋颖), Qiuyun Chen(陈秋云), Wei Feng(冯卫), Xiangfei Yang(杨向飞), Qin Liu(刘琴), Xiegang Zhu(朱燮刚), Dengpeng Yuan(袁登鹏), Qiang Zhang(张强), Xinchun Lai(赖新春), Qunqing Hao(郝群庆), and Shiyong Tan(谭世勇)

Citation: Chin. Phys. B, 2026, 35 (**4**): 047102. DOI: 10.1088/1674-1056/ae101a
http://cpb.iphy.ac.cn; http://iopscience.iop.org/cpb

What follows is a list of articles you may be interested in

Electronic structure study of the intermetallic compound $GdRhIn_5$

Yulu He(贺宇璐), Bo Wang(王博), Xiangfei Yang(杨向飞), Dengpeng Yuan(袁登鹏), Wei Feng(冯卫), Yaobo Huang(黄耀波), and Qiuyun Chen(陈秋云)

Chin. Phys. B, 2026, 35 (**3**): 037101. DOI: 10.1088/1674-1056/ae3123

Ab initio prediction of ground-state magnetic ordering and high-pressure magnetic phase transition of uranium mononitride

Jing-Jing Zheng(郑晶晶), Yuxi Chen(陈禹西), Chengxiang Zhao(赵承祥), Junfeng Zhang(张均锋), Ping Zhang(张平), Bao-Tian Wang(王保田), and Jiang-Jiang Ma(马江将)

Chin. Phys. B, 2025, 34 (**8**): 087101. DOI: 10.1088/1674-1056/add4e6

Site selective 5f electronic correlations in *β*-uranium

Ruizhi Qiu(邱睿智), Liuhua Xie(谢刘桦), and Li Huang(黄理)

Chin. Phys. B, 2023, 32 (**1**): 017101. DOI: 10.1088/1674-1056/ac76ad

Effect of strain on charge density wave order in α-U

Liuhua Xie(谢刘桦), Hongkuan Yuan(袁宏宽), and Ruizhi Qiu(邱睿智)

Chin. Phys. B, 2022, 31 (**6**): 067103. DOI: 10.1088/1674-1056/ac4f4d

First-principles calculation of the electronic structure, chemical bonding, and thermodynamic properties of *β*-US_2

Li Shi-Chang (李世长), Zheng Yuan-Lei (郑远蕾), Ma Sheng-Gui (马生贵), Gao Tao (高涛), Ao Bing-Yun (敖冰云)

Chin. Phys. B, 2015, 24 (**12**): 127101. DOI: 10.1088/1674-1056/24/12/127101

Fine electronic structure and 5f-electron localized–itinerant transition in uranium films

Yun Zhang(张云)[†], Jian Wu(吴健)[†], Ying Jiang(蒋颖)[†], Qiuyun Chen(陈秋云), Wei Feng(冯卫), Xiangfei Yang(杨向飞), Qin Liu(刘琴), Xiegang Zhu(朱燮刚), Dengpeng Yuan(袁登鹏), Qiang Zhang(张强), Xinchun Lai(赖新春), Qunqing Hao(郝群庆)[‡], and Shiyong Tan(谭世勇)[§]

National Key Laboratory of Surface Physics and Chemistry, Mianyang 621908, *China*

(Received 18 July 2025; revised manuscript received 8 September 2025; accepted manuscript online 7 October 2025)

Uranium, the heaviest natural element, exhibits rich and complex physical behavior, including three types of charge density wave transitions and superconductivity at low temperatures. It is widely believed that these phenomena are closely linked to the properties of 5f electrons, which are highly susceptible to external perturbations. To elucidate the detailed electronic structure, particularly the 5f electron signatures, we fabricated high-quality single-crystal uranium films on W (110) substrates using molecular beam epitaxy and investigated their fine electronic properties and temperature-dependent evolution by angle-resolved photoemission spectroscopy (ARPES). Our experiments reveal three electron pockets around the Γ point and direct hybridization between 5f electrons and conduction electrons at regions distant from Γ. The Kondo temperature extracted from ARPES and electrical resistance measurements is approximately 131 K, indicating that the 5f electrons transition from a high-temperature localized state to a low-temperature itinerant state in the thin film system. Additionally, we observe another flat band with an energy scale of 148 meV. The detailed electronic structure and direct evidence of the localized-to-itinerant transition of 5f electrons provided in this study advance the understanding of strong electronic correlations in uranium-based materials.

Keywords: uranium, c–f hybridization, Kondo physics

PACS: 71.27.+a , 73.20.At, 79.60.–i

DOI: 10.1088/1674-1056/ae101a **CSTR:** 32038.14.CPB.ae101a

1. Introduction

Uranium, the heaviest natural element, has been extensively utilized in engineering applications for large-scale energy production. Beyond its practical uses, it also exhibits a range of remarkable quantum phenomena in the realm of condensed matter physics,[1] including multiple complex charge density wave (CDW) states[2] and ambient-pressure superconductivity at low temperatures.[3] Uranium undergoes three distinct CDW transitions — denoted as α_1, α_2, and α_3 phases — below critical temperatures of 42 K, 36 K, and 23 K, respectively. Upon further cooling, it goes into a superconducting state below 2 K. Subsequent experimental studies revealed that high-quality uranium crystals with well-developed CDW states do not exhibit superconductivity, suggesting a mutual exclusion between the CDW and superconducting orders.[4] The evolution of the CDW states and their interplay with superconductivity remain unclear and require further investigation. Given that most of these intriguing properties are intimately linked to uranium's electronic structure, a detailed understanding of its electronic properties is essential for deciphering the underlying mechanisms of these complex physical behaviors.

A pivotal issue in the study of uranium concerns the role of 5f electrons in governing its physical properties. As is well known, the spatial extension of 5f orbitals leads to considerable overlap between adjacent sites, resulting in relatively broad 5f bands. These 5f electrons behave quite differently from the more localized 4f electrons found in rare-earth systems, which typically exhibit localized character at high temperatures and become itinerant upon cooling — a phenomenon central to Kondo physics. In uranium, the ground state above the CDW transition is paramagnetic,[5] with a small localized magnetic moment of approximately 0.04 μ_B observed in bulk α-uranium. Moreover, the electronic specific heat coefficient suggests that uranium is a moderate-effective-mass system.[2] Whether such a modest magnetic moment and a specific heat coefficient of this material can give rise to Kondo behavior analogous to that in 4f electron systems remains an open question. Nevertheless, several studies[6,7] have indicated that hybridization between 5f and conduction electrons may still occur in uranium.

The situation may differ markedly at the surface compared with bulk materials. Computational studies predict a significantly enhanced magnetic moment of about 0.65 μ_B on the (001) surface of uranium.[8] This pronounced increase in surface magnetism could substantially strengthen Kondo cor-

[†]These authors contributed equally to this work.

[‡]Corresponding author. E-mail: qunqinghao@163.com

[§]Corresponding author. E-mail: sytan4444@163.com

© 2026 Chinese Physical Society and IOP Publishing Ltd. All rights, including for text and data mining, AI training, and similar technologies, are reserved.

relations under certain conditions. We therefore suggest that a stark contrast likely exists between the bulk and surface electronic behaviors of uranium, making this distinction a particularly compelling direction for future research. Indeed, the f electrons in Kondo lattice compounds are highly susceptible to external perturbations, such as pressure, temperature, chemical doping, and magnetic fields.[9–15] Further refined experimental characterization, such as temperature-dependent experiments, is essential to elucidate their behavior and resolve outstanding questions in this complex system.

To clarify these issues, the first essential step is the preparation of high-quality single crystals. Bulk single-crystal uranium samples are mechanically soft and difficult to cleave. Conventional surface preparation techniques, such as sputtering and annealing, often fail to yield atomically smooth and contamination-free surfaces. These limitations pose significant challenges for precise electronic structure characterization. In contrast, thin films of uranium offer distinct advantages, including superior surface flatness and well-controlled synthesis conditions. Consequently, numerous studies have focused on investigating the electronic properties of uranium thin films.[16–22]

Angle-resolved photoemission spectroscopy (ARPES) is a powerful technique for probing the electronic structure of materials.[23–25] Previous ARPES studies on high-quality bulk uranium and single-crystal thin films have revealed fundamental band structures and 5f-electron characteristics.[7,26,27] Complementary scanning tunneling microscopy/spectroscopy measurements further confirmed that the density of states near the Fermi level is dominated by 5f electrons.[20] However, due to limitations in sample quality and instrumental energy resolution, detailed investigations into the fine electronic structure and temperature-dependent evolution of 5f states have remained scarce.

In this study, we successfully synthesized high-quality single-crystal uranium films on W(110) substrates. Using ARPES, we systematically investigated the Fermi surface topology, valence band structure, and temperature-dependent band evolution. Our results reveal a direct hybridization between 5f electrons and conduction electrons far from the Γ point. We determined a Kondo temperature of approximately 131 K for the 5f electrons in the uranium film and identified an additional flat band with an energy scale of 148 meV. Electrical resistance measurements further support the presence of Kondo lattice behavior. These findings provide key insights into the complex and tunable electronic properties of uranium at low temperatures.

2. Experiments and computations

Sample preparations MBE and ARPES experiments were performed in an interconnected ultrahigh vacuum (UHV) system with a base pressure maintained below 8×10^{-11} mbar. Prior to the epitaxial growth of uranium thin films, the W(110) single-crystal substrate underwent successive cycles of Ar^+ sputtering and annealing to eliminate surface contaminants and defects. It was subsequently annealed at approximately 1200 K and then rapidly cooled to room temperature to achieve an atomically smooth surface. Uranium films were deposited on the prepared substrate using a deflection electron beam evaporator. High-purity (99.9%) uranium metal was degassed by heating for over two weeks within the MBE chamber before initial deposition. The evaporation rate, monitored by a quartz crystal microbalance, was maintained at approximately 0.10 Å/s for all samples studied. Throughout the deposition process, the substrate was held at room temperature. The crystallographic quality and surface structure of the uranium films were characterized *in situ* by low-energy electron diffraction (LEED).

ARPES and PPMS measurements Electrical transport measurements were carried out using a quantum design physical property measurement system (PPMS). The electronic structures of the uranium films were investigated by ARPES utilizing a helium discharge lamp (He-Iα, $h\nu = 21.2$ eV) with a beam spot size of approximately 1 mm. All ARPES data were acquired with a Scienta R4000 electron analyzer, achieving an energy resolution of 10 meV or better and an angular resolution better than 0.2°. The Fermi level (E_F) was referenced by measuring *in-situ* deposited gold films. For ARPES measurements, uranium films with a thickness of about 20 nm were utilized, while a thicker film of approximately 100 nm, deposited on insulating Al_2O_3 substrates, was employed for the electrical transport measurements in the PPMS.

Computational methodology The primitive cell of α-U contains two uranium atoms with atomic coordinates at (0.099, 0.901, 0.25) and (0.901, 0.099, 0.75), as shown in Figs. 1(a) and 1(b). Since the prepared α uranium thin films exhibit (001) surfaces, we constructed an α-U (001) surface model containing 17 uranium atoms with symmetric upper and lower surfaces. A vacuum layer of 15 Å was introduced on the upper and lower surfaces, as illustrated in Fig. 1(c). The electronic structure of α-U (001) was calculated using the Vienna *ab initio* simulation package (VASP)[28–30] with the projector augmented wave method.[31] The exchange–correlation potential was described by the Perdew–Burke–Ernzerhof functional[32] within the generalized gradient approximation (GGA). The plane-wave cutoff energy was set to 500 eV, and the Brillouin zone was sampled using a Γ-centered scheme with a $13\times13\times1$ k-point mesh. Convergence tests were performed to verify the total energy convergence with respect to cutoff energy and k-point mesh density. The energy tolerance for the electronic self-consistent loop convergence was set to 1.0×10^{-8} eV. Surface atomic relaxation was performed us-

ing the conjugate gradient method (with four uranium atoms each on the upper and lower surfaces, as indicated by the light blue spheres in Fig. 1(c)) until the Hellmann–Feynman force on each atom was less than 0.01 eV/Å. Considering the strong correlation effects in uranium systems, the GGA + U method[33] was employed for electronic structure calculations after surface relaxation. The effective Coulomb interaction parameter U for α-U was set to 4.0 eV based on our previous study.[34]

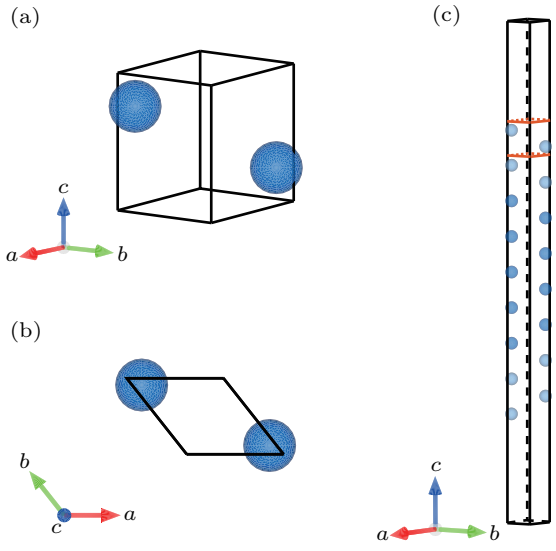


Fig. 1. (a) Side and (b) top views of the primitive cell of α-uranium. (c) Side view of α-U (001) surface model, the primitive cell unit is marked by orange lines. Light blue spheres indicate surface uranium atoms participating in surface relaxation, whereas dark blue spheres correspond to bulk uranium atoms held fixed during calculations.

3. Results

The single crystal uranium thin films on W(110) substrate are prepared with MBE method. The sharp and clear LEED pattern of the as-grown uranium thin films as shown in Fig. 2(a) indicates the high quality of the thin films. The LEED pattern is fully consistent with the diffraction pattern for orthorhombic α-U(001) crystallographic structure (space group *Cmcm*, No. 63) at room temperature, indicating the surface structure of the deposited film is α-U(001). The lattice constants of α-U are $a = 3.2$ Å, $b = 3.2$ Å and $c = 4.96$ Å. However, the LEED pattern is superimposed by two sets of identical lattice structures. This phenomenon results from the two types of domains in the as-grown uranium thin films. Initially, the evaporated U atoms deposit at the long bridge sites of W(110), which exhibit the lowest adsorption energy. The subsequent deposited U atoms can relax in two directions to release the stress, leading to the formation of two domains.[34] Even if there are two domains on the deposited film, the electronic structure does not change significantly. There are two reasons for this: first, our previous measurements proved that there is only a 3° rotation between the two domains,[34] such a small rotation cannot affect the electronic structure too much; second, the information from the LEED pattern in Fig. 2(a) indicates that there is a significant difference in the proportion of the two domains. The electronic structure of the thin film is dominated by the domain with a higher proportion, corresponding to the brighter diffraction points. The Fermi surface topology of uranium thin film is displayed in Figs. 2(d) and 2(e). The fine electronic structure contains more information than the previous report.[7]

High-quality single-crystal uranium thin films were grown on W(110) substrates using molecular beam epitaxy (MBE). The sharp and well-defined LEED pattern presented in Fig. 2(a) demonstrates the high crystalline quality of the deposited film. The observed LEED pattern is fully consistent with the orthorhombic α-U(001) structure (space group *Cmcm*, No. 63) at room temperature, confirming the formation of α-phase uranium with lattice parameters $a = 3.2$ Å, $b = 3.2$ Å, and $c = 4.96$ Å. The LEED image exhibits a superposition of two identical lattice patterns, which arises from the presence of two distinct domains within the uranium film. During the initial growth stage, uranium atoms adsorb preferentially at the long-bridge sites of the W(110) surface, which exhibit the lowest adsorption energy. Subsequent atomic deposition leads to stress relaxation along two symmetric directions, resulting in the formation of two rotational domains.[34] Despite this domain structure, the electronic properties of the film remain largely unaffected, for two main reasons: first, previous measurements have shown that the two domains are rotated by only 3° after mirror symmetry relative to each other,[34] which is insufficient to induce significant electronic modifications; second, the LEED pattern in Fig. 2(a) reveals a substantial disparity in the domain populations, implying that the electronic structure is dominated by the majority domain corresponding to the brighter diffraction spots. The Fermi surface topology of the uranium thin film is presented in Figs. 2(d) and 2(e). These results reveal fine electronic structural details that offer substantially more information than previously reported data.[7]

To further elucidate the electronic properties of the uranium thin films, we performed electrical resistance measurements on samples deposited on insulating Al_2O_3 substrates, as shown in Fig. 2(b). In the absence of a magnetic field, the resistivity decreases with decreasing temperature, confirming metallic behavior. Notably, a distinct slope change is observed in the resistance-temperature curve between 100 K and 150 K, a feature commonly found in heavy-fermion compounds containing f electrons.[11,35] In such systems, this anomaly is attributed to the transition of f electrons from a high-temperature localized state to a low-temperature itinerant state. At high temperatures, the f electrons remain localized; upon cooling, they hybridize with conduction electrons, forming heavy

quasiparticles with enhanced effective mass. Compared to bulk uranium,[36] the slope change in our thin films is more pronounced, likely due to an enhanced local moment and Kondo effect in the thin film form. Furthermore, resistance measurements under magnetic fields up to 8 T reveal no significant change in the temperature-dependent behavior, indicating that the electronic transport in these uranium films is largely insensitive to magnetic fields.

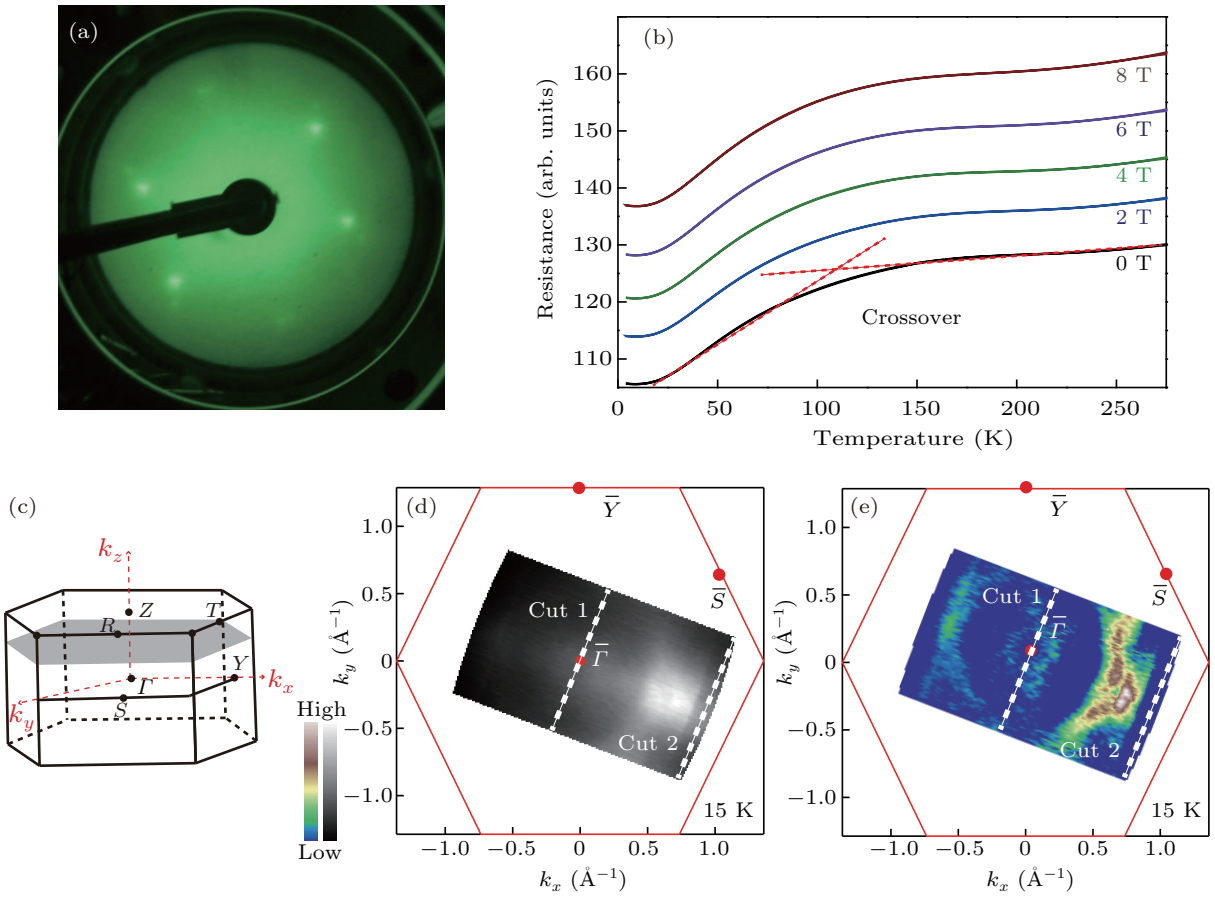


Fig. 2. The surface lattice structure, the resistance measurements, Brillouin zone, and Fermi surface topology of the uranium thin films. (a) LEED pattern of the as-grown uranium film. (b) Temperature-dependent electrical resistance of uranium thin films under various magnetic fields (0 T to 8 T). Data are vertically offset for clarity. The intersection of the red dashed lines indicates the crossover region. (c) Brillouin zone and k_z cut calculated for a photon energy of 21.2 eV using an inner potential of 15 eV (gray plane). (d) Fermi surface mapping at 15 K, integrated within an energy window of $E_F \pm 10$ meV. (e) Curvature representation of the Fermi surface shown in panel (d).

To elucidate the fine electronic structure of the uranium thin films, we present a detailed characterization of their valence band spectrum in Fig. 3. As shown in Figs. 3(a) and 3(b), three electron-like bands — denoted as α, β, and γ — are clearly resolved. The bottom of the α band is situated at approximately 50 meV binding energy, while the β and γ bands both bottom out near 300 meV. A pronounced hybridization feature appears at around 1.5 eV binding energy, where an electron-like band interacts with a hole-like band, resulting in the opening of a hybridization gap. Notably, no flat band is observed near the Γ point. The angle-integrated photoemission spectrum in Fig. 3(a2) exhibits three distinct peaks labeled a, b, and c, located at -50 meV, -300 meV, and -1 eV, respectively. Peak a corresponds to the α band, while peak b comprises contributions from both the β and γ bands. Peak c originates from a deeper-lying energy band.

Moving away from the Γ point along cut 2, a weakly dispersive band is observed near the Fermi level. This band hybridizes with two hole-like bands, labeled δ and ε. The angle-integrated spectrum in Fig. 3(c2) reveals a pronounced density of states close to the Fermi level, resembling features commonly associated with f-electron states in heavy-fermion systems.[14] If this weakly dispersive band indeed originates from f electrons, it would be expected to exhibit localized character at high temperatures and gradually hybridize with conduction electrons as the temperature decreases. Such hybridization typically leads to the emergence of a quasiparticle peak near the Fermi energy.[14,37] To confirm the f-electron nature of this state, further variable-temperature ARPES experiments are necessary.

In addition, a flat band is observed at a binding energy of 148 meV in Figs. 3(c1) and 3(c2). This feature resembles flat bands commonly found in other f-electron systems, which often arise from crystal field effects or spin–orbit coupling.[37–39]

In such systems, these interactions can split f-electron bands into multiple flat subbands. In light actinides, the energy scale of spin–orbit coupling typically far exceeds that of the crystal field effect.[40] For uranium 5f electrons, the spin–orbit coupling strength is approximately 250–300 meV,[40,41] whereas the crystal field splitting is on the order of 100 meV.[41] Given that the observed flat band lies at 148 meV — significantly lower than typical spin–orbit coupling energies but consistent with crystal field splitting — we propose that this feature likely originates from crystal field effects rather than spin–orbit coupling. However, to unambiguously determine the origin of this flat band, further experimental investigations using techniques such as neutron diffraction are warranted.

To elucidate the origin of the electronic structure in uranium thin films, we conducted time-dependent comparative experiments, as summarized in Fig. 4. Figure 4(a) displays the well-resolved band structure of a freshly deposited uranium film, details of which are provided in Fig. 3. Owing to the high chemical reactivity of uranium, significant changes in the electronic structure are observed after the film remains in the UHV chamber for three hours (base pressure better than 5×10^{-11} mbar), as shown in Fig. 4(b). The bands near the Fermi level exhibit noticeable broadening and reduced clarity compared to those in the as-deposited sample, whereas bands at higher binding energies (below 1.5 eV) remain unchanged aside from minor broadening and a slight attenuation of band c. This evolution is clearly visible in the angle-integrated spectra in Fig. 4(c). Both bands a and b become broader, with band a also showing slight intensity reduction. The most pronounced change occurs in band b, which weakens considerably. This distinct sensitivity of band b to aging — contrasting with the relative stability of other features — suggests that it may possess distinct electronic properties. Given that the sample was kept under UHV conditions, the observed changes are likely due to interaction with trace residual gases (e.g., hydrogen), implying that band b may be particularly susceptible to physical adsorption or mild surface reactions.

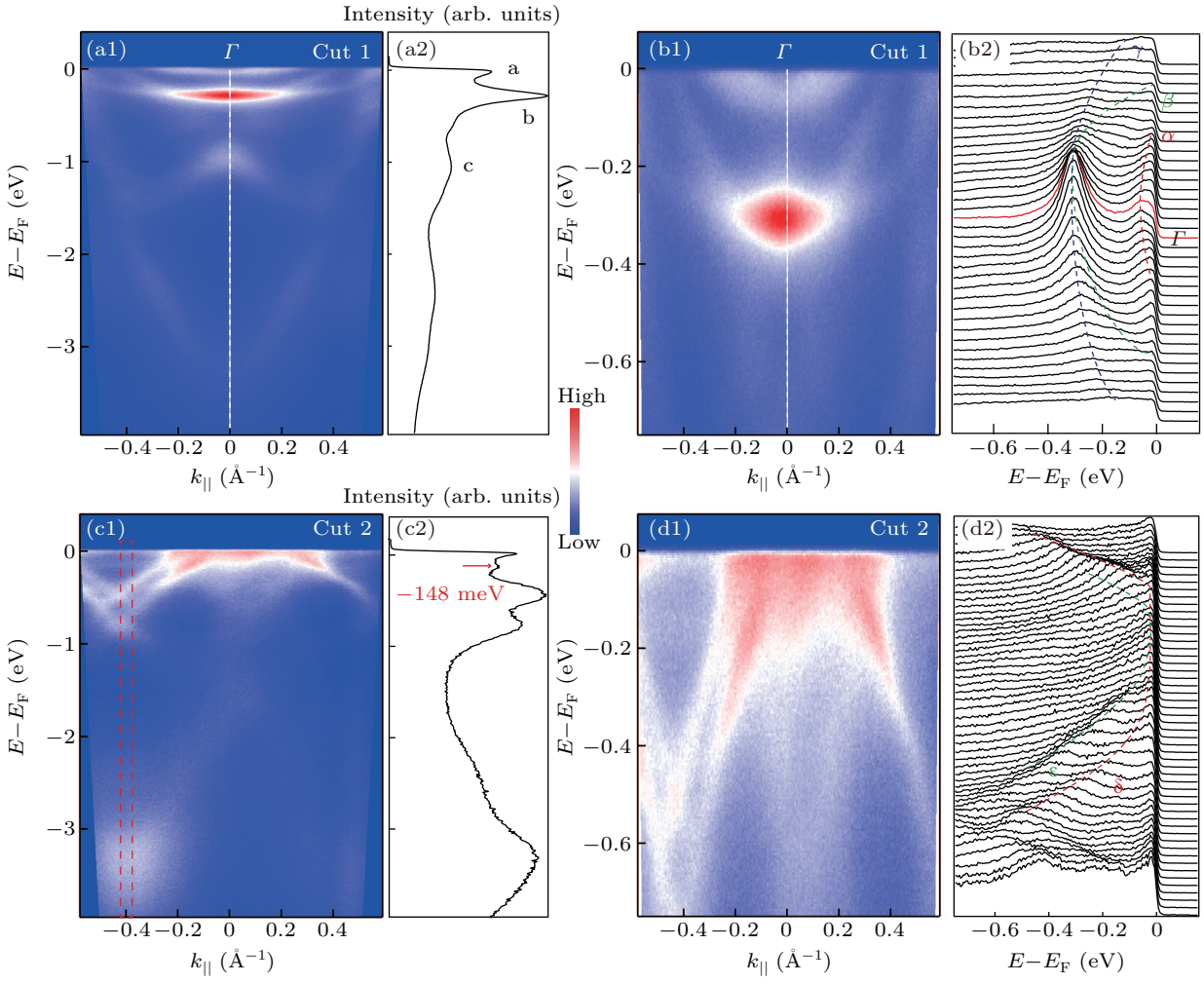


Fig. 3. Fine electronic structure of the uranium thin film. (a1) Band structure measured along cut 1 (defined in Fig. 2(d)) over a wide energy range. (a2) Corresponding angle-integrated photoemission spectrum integrated over the momentum range from −0.5 Å^{-1} to 0.5 Å^{-1}. (b1)–(b2) High-resolution band structure along cut 1 (as shown in Fig. 2(d)) near the Fermi level and the corresponding energy distribution curves (EDCs). (c1)–(c2) Band structure and angle-integrated spectrum along cut 2 (Fig. 2(d)). The integration region for (c2) is indicated by the red dashed rectangle in panel (c1). (d1)–(d2) Magnified view of the band structure and EDCs along cut 2 within the same energy window as (b1)–(b2).

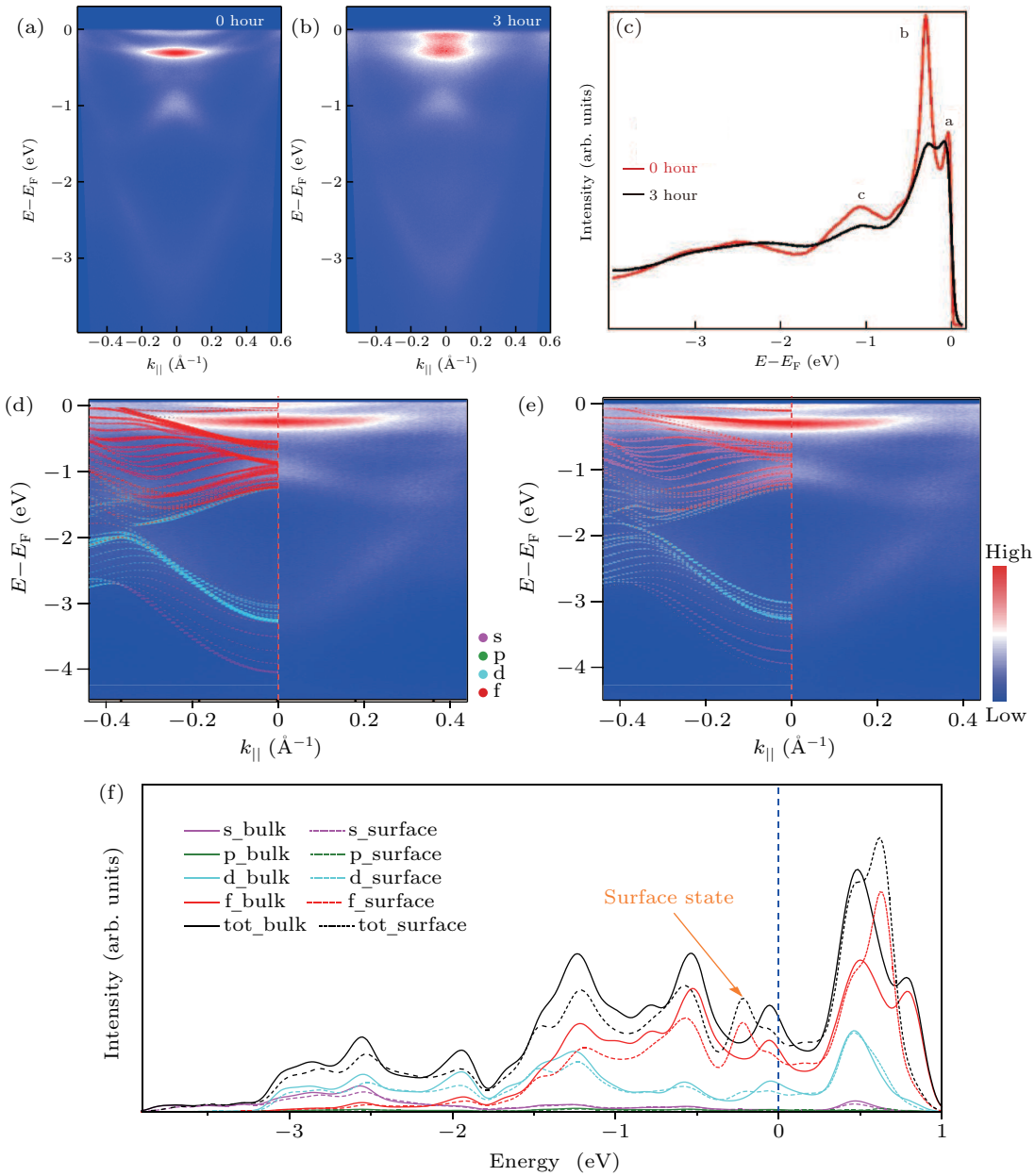


Fig. 4. Experimental and theoretical electronic structures of the uranium thin film. (a) Band structure of the film immediately after deposition. (b) Band structure after three hours of measurement. (c) Angle-integrated photoemission spectra corresponding to (a) and (b), integrated over the range from -0.5 Å^{-1} to 0.5 Å^{-1}. (d) Experimental photoemission intensity map overlaid with the calculated bulk-projected band structure. The colored dots indicate orbital contributions: magenta (s), olive (p), cyan (d), and red (f). (e) Same as (d) but for the surface-projected band structure. (f) Orbital-projected density of states for uranium. Solid lines represent the bulk-projected values, while dashed lines correspond to the surface-projected case.

To clarify the origin of those bands, we also calculated the band structures of the uranium thin film. We first conducted a spatial band projection analysis for the intermediate-layer atoms to represent the bulk band structure of α-uranium. For direct comparison, these bands were superimposed on the photoemission intensity map as shown in Fig. 4(d). The band structure of the intermediate atoms resembles the bulk band structure, and all experimentally observed bands in the photoemission intensity map exhibit corresponding calculated bands, except the band at 300 meV binding energy, as illustrated in Fig. 4(d). From the calculation results, the electronic structure below 2 eV binding energy is dominated by the p, d, and s orbitals, while the bands near the Fermi level are mainly dominated by f electrons. However, the band at 300 meV binding energy is missing in the calculated results, as illustrated in Fig. 4(d). From experimental evidence as shown in Fig. 4(c), it has been confirmed that band b is not consistent with other band properties, and the bulk-projected band cannot reproduce band b. Therefore, we consider whether band b is contributed by surface states.

To confirm whether the band b is a surface state, we further conduct a spatial band projection analysis for the surface atoms (four atoms each on the upper and lower surfaces), corresponding to the surface bands of α-uranium. These bands

were also superimposed on the photoemission intensity map, as shown in Fig. 4(e). For the surface atoms, the intensity of projected bands at higher binding energy weakens compared with the bulk-projected band structures, but a prominent band near 300 meV binding energy emerges, matching well with the 300 meV binding energy band feature in the photoemission intensity map. This confirms that the band at 300 meV binding energy in the photoemission intensity map is a surface state and can only be found on surface atoms. Projected partial wave density of states analysis reveals that this surface state mainly originates from f electrons, with a small amount of d electron features as shown in Fig. 4(f). This explains why band b is highly susceptible to environmental influences. The electrons associated with band b are located exclusively on the surface of the uranium thin film, where they are directly exposed to and interact with atmospheric conditions.

To determine whether the weakly dispersive band in Fig. 3(d) is of f-electron character, variable-temperature experiments were performed on uranium films, as shown in Fig. 5(a). At 10 K, this weakly dispersive band hybridizes with two hole-like bands and exhibits strong intensity. As the temperature increases to 300 K, the band broadens noticeably. Upon cooling back to 10 K, the band sharpens again, confirming that its temperature-dependent evolution is an intrinsic property rather than an effect of sample aging. Figure 5(b) presents the temperature-dependent band structures after subtraction of the Fermi–Dirac distribution, revealing a distinct flat band near the Fermi level that broadens with increasing temperature. It is noteworthy that these measurements were conducted at a photon energy of 21.2 eV. Although the photoemission cross-section for uranium is highest for 6d electrons, not 5f electrons,[42] the measured density of states of the f-electrons under these conditions still exceeds that of the other conduction electrons. This indicates that in α-uranium, the true density of 5f electronic states near the Fermi level is significantly higher than that of other conduction electrons, in good agreement with theoretical calculations presented in Fig. 4.

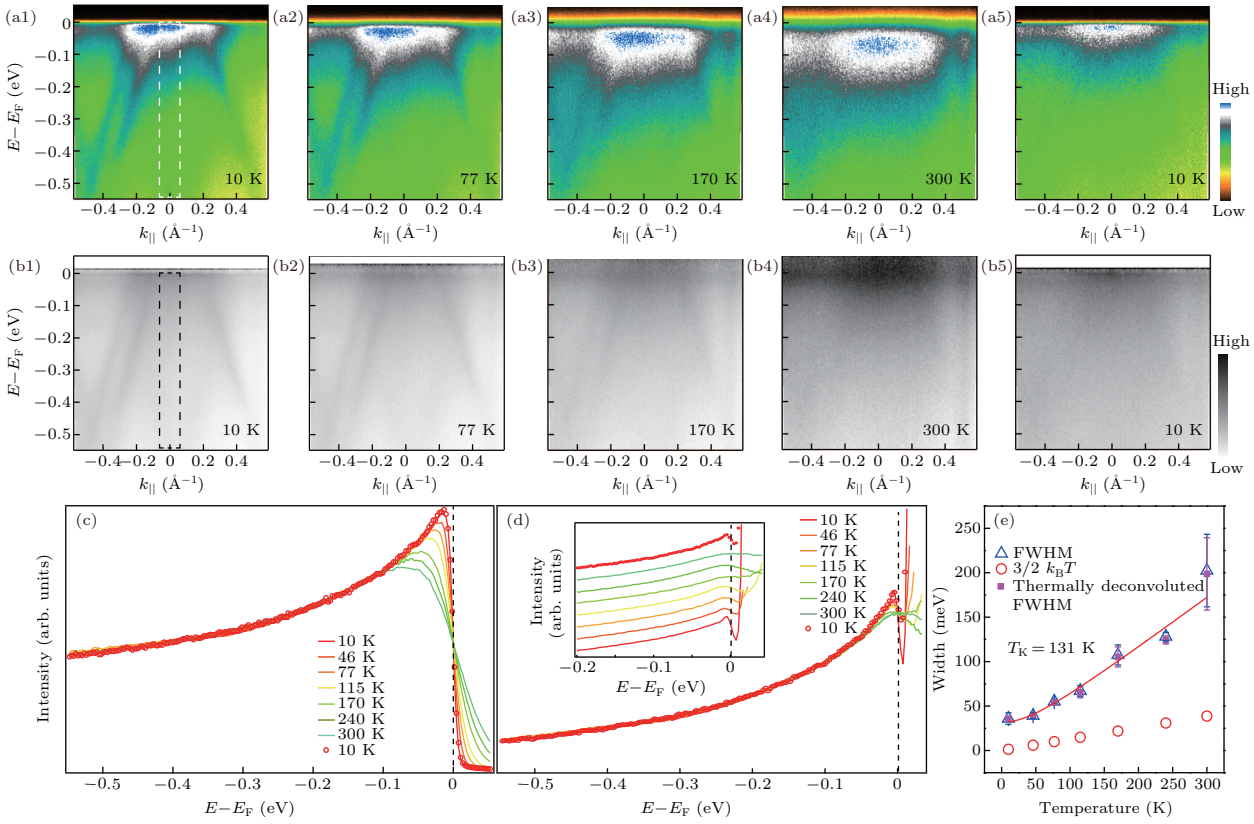


Fig. 5. Variable-temperature band structures of the uranium thin film. (a1)–(a5) Evolution of the band structure of the α-uranium film along cut 2 (defined in Fig. 2(d)) as a function of temperature. Results from (a1) to (a4) correspond to a heating process from 10 K to 300 K, while (a5) shows the band structure recorded during cooling from 300 K back to 10 K. The same sample was used throughout all measurements in (a1)–(a5). (b1)–(b5) Band structures obtained after subtracting the Fermi–Dirac distribution at each corresponding temperature in panels (a1)–(a5). (c) Angle-integrated photoemission spectra derived from the bands shown in (a) at various temperatures. The angular integration region is indicated by the dashed rectangle in panel (a1). (d) Angle-integrated photoemission spectra corresponding to the bands in panel (b) at different temperatures. The angular integration region is indicated by the dashed rectangle in panel (b1). Curves are vertically offset for clarity (see inset). Spectral fitting was performed using the formula $[y = y_0 + \frac{A}{\pi/2} \times \frac{w}{4(x-x_c)^2+w^2}]$, where x_c denotes the peak position and w represents the peak width, within the energy range from -0.05 eV to 0.01 eV. Intensity curves in panels (c) and (d) were normalized by aligning all spectra at a binding energy of 0.55 eV. (e) Evolution of the full width at halfmaximum (FWHM) obtained from fitting the peaks near the Fermi level in panel (d). Blue triangles correspond to the FWHM of the f-electron peak shown in panel (d); red circles represent the thermal broadening component; purple squares indicate the FWHM after subtracting thermal broadening; the red curve shows a fit based on the Kondo model.

To gain further insight into the evolution of the flat band, the corresponding angle-integrated photoemission spectra are presented in Figs. 5(c) and 5(d). The momentum integration range used for these spectra was limited to ± 0.07 Å^{-1}, intentionally avoiding integration over the conduction electron bands. This approach ensures that the spectral features primarily reflect the f-electron contributions. In addition to thermal broadening, the intensity of the f-electron band is also suppressed with increasing temperature and recovers upon cooling, further confirming that the temperature-dependent evolution of the density of states is an intrinsic effect. This behavior aligns with the f-electron characteristics observed in other heavy-fermion systems.[14,15]

As clearly observed in Fig. 5(d), the f-electron spectral weight evolves systematically with temperature. Subtraction of the Fermi–Dirac distribution allows partial access to the unoccupied electronic structure above the Fermi level, yielding a more complete picture of the flat band. We find that the width of the flat band increases with temperature, and its line shape is well described by a Lorentzian function.

Accordingly, the FWHM of the flat band peak, derived from Lorentzian fits to the spectra in Fig. 5(d), is presented in Fig. 5(e). After accounting for thermal broadening, the intrinsic temperature-dependent FWHM of the f-electron density of states is obtained. The results reveal significant broadening of the flat band with increasing temperature.

Actually, in the f-electron system, results for the single-channel spin one-half Kondo impurity model in a Fermi liquid regime have been used to describe the temperature dependence of the FWHM,[43,44] as shown by the following formula:

$$\mathrm{FWHM} = 2\sqrt{(\pi k_{\mathrm{B}} T)^2 + 2(k_{\mathrm{B}} T_{\mathrm{K}})^2}, \tag{1}$$

where k_{B} is the Boltzmann constant, and T_{K} is the Kondo temperature of materials. The excellent agreement between the FWHM and the fitting formula confirms the f-electron nature of the flat band. Furthermore, the fit yields a Kondo temperature of 131 K for α-uranium, which is consistent with the crossover temperature observed in electrical resistance measurements, as shown in Fig. 2(b).

4. Discussion and conclusion

Previous scanning tunneling spectroscopy studies have revealed a Kondo resonance peak near the Fermi level at low temperatures in uranium thin films thicker than four atomic monolayers.[45] This observation indicates that Kondo behavior, and the associated formation of a coherent electronic state, emerges in α-uranium when the film exceeds this critical thickness.

Demonstrating Kondo lattice behavior in a material system is inherently challenging and typically requires convergent evidence from multiple experimental techniques. In the case of the α-uranium thin film, our conclusions are supported by several key observations. First, temperature-dependent electronic structure measurements reveal a flat band that weakens and broadens with increasing temperature. Notably, the rate of this spectral evolution significantly exceeds simple thermal broadening and is instead well described by a Kondo impurity model, as shown in Fig. 5, providing strong evidence that the flat band originates from the hybridized f-electrons. Second, the electrical resistance-temperature curve exhibits characteristics consistent with Kondo lattice behavior, as seen in Fig. 2(b). Third, these findings are further corroborated by prior experimental and theoretical studies.[6,7,45] In particular, the enhanced surface local moments in this thin film system[8] may play a critical role in enabling the emergence of Kondo physics. Taken together, these results strongly support the presence of Kondo behavior in α-uranium.

Since α-uranium is a single-element metal, a key question concerns which conduction electrons hybridize with the 5f electrons. According to the computational results in Fig. 4(f), the density of states near the Fermi level is dominated by f- and d-electrons, with their spectral shapes and peak positions showing strong agreement. This indicates that hybridization in uranium films occurs primarily between 5f and 6d electrons. In comparison to 4f electron systems,[46,47] the 5f electrons exhibit a broader bandwidth. Nevertheless, both systems display a temperature-driven transition from localized to itinerant electronic behavior.

In summary, high-quality single-crystal α-uranium films were grown on W(110) substrates using MBE. Their electronic properties, including Fermi surface topology, valence band structure, and temperature-dependent band evolution, were systematically investigated using ARPES. Three electron pockets were observed around the Γ point, while no f-electron band was detected in this region. Instead, direct hybridization between f-electrons and conduction electrons was identified at momenta far from Γ. Variable-temperature ARPES measurements revealed a Kondo temperature of approximately 131 K in the uranium films. Additionally, a flat band with an energy scale of 148 meV was observed. These results provide detailed electronic structure characterization and confirm the presence of Kondo physics in α-uranium, contributing to a deeper understanding of strong electron correlations in uranium-based systems.

Acknowledgments

Project supported by the National Key Research and Development Program of China (Grant Nos. 2021YFA1601101 and 2022YFA1402201), the National Natural Science Foundation of China (Grant Nos. 52394161 and

U2430209), Sichuan Science & Technology Program (Grant No. 2025ZNSFSC0869), and the Institute of Materials (Grant No. TP02202408).

References

[1] Lander G H, Fisher E S and Bader S D 1994 *Adv. Phys.* **43** 1

[2] Lashley J C, Lang B E, Boerio-Goates J, Woodfield B F, Schmiedeshoff G M, Gay E C, McPheeters C C, Thoma D J, Hults W L, Cooley J C, Hanrahan R J Jr and Smith J L 2001 *Phys. Rev. B* **63** 224510

[3] Fowler R D, Lindsay J D G, White R W, Hill H H and Matthias B T 1967 *Phys. Rev. Lett.* **19** 892

[4] Graf D, Stillwell R, Murphy T P, Park J H, Kano M, Palm E C, Schlottmann P, Bourg J, Collar K N, Cooley J C, Lashley J C, Willit J and Tozer S W 2009 *Phys. Rev. B* **80** 241101

[5] Ross J W and Lam D J 1968 *Phys. Rev.* **165** 617

[6] Yang X and Riseborough P S 2010 *Phys. Rev. B* **82** 094303

[7] Chen Q, Tan S, Feng W, Luo L, Zhu X and Lai X 2019 *Chin. Phys. B* **28** 077404

[8] Stojić N, Davenport J W, Komelj M and Glimm J 2003 *Phys. Rev. B* **68** 094407

[9] Santander-Syro A F, Klein M, Boariu F L, Nuber A, Lejay P and Reinert F 2009 *Nat. Phys.* **5** 637

[10] Si Q and Steglich F 2010 *Science* **329** 1161

[11] Hegger H, Petrovic C, Moshopoulou E G, Hundley M F, Sarrao J L, Fisk Z and Thompson J D 2000 *Phys. Rev. Lett.* **84** 4986

[12] Aynajian P, da Silva Neto E H, Gyenis A, Baumbach R E, Thompson J D, Fisk Z, Bauer E D and Yazdani A 2012 *Nature* **486** 201

[13] Ruan W, Ye C, Guo M, Chen F, Chen X, Zhang G and Wang Y 2014 *Phys. Rev. Lett.* **112** 136401

[14] Chen Q Y, Xu D F, Niu X H, Jiang J, Peng R, Xu H C, Wen C H P, Ding Z F, Huang K, Shu L, Zhang Y J, Lee H, Strocov V N, Shi M, Bisti F, Schmitt T, Huang Y B, Dudin P, Lai X C, Kirchner S, Yuan H Q and Feng D L 2017 *Phys. Rev. B* **96** 045107

[15] Chatterjee S, Trinckauf J, Hänke T, Shai D E, Harter J W, Williams T J, Luke G M, Shen K M and Geck J 2013 *Phys. Rev. Lett.* **110** 186401

[16] Gouder T and Colmenares C A 1993 *Surf. Sci.* **295** 241

[17] Springell R, Bright E L, Chaney D A, Harding L M, Bell C, Ward R C C and Lander G H 2022 *Adv. Phys.* **71** 87

[18] Gouder T, Colmenares C A and Naegele J R 1995 *Surf. Sci.* **342** 299

[19] Fujimori S, Saito Y, Yamaki K, Okane T, Sato N, Komatsubara T, Suzuki S and Sato S 2000 *Surf. Sci.* **444** 180

[20] Berbil-Bautista L, Hänke T, Getzlaff M and Wiesendanger R 2004 *Phys. Rev. B* **70** 113401

[21] Springell R, Detlefs B, Lander G H, Ward R C C, Cowley R A, Ling N, Goetze W, Ahuja R, Luo W and Johansson B 2008 *Phys. Rev. B* **78** 193403

[22] Fujimori S, Saito Y, Ejima T, Sato N, Komatsubara T, Kunii S, Suzuki S, Sato S and Ishii T 1996 *J. Electron Spectrosc.* **78** 155

[23] Richard P, Nakayama K, Sato T, Neupane M, Xu Y M, Bowen J H, Chen G F, Luo J L, Wang N L, Dai X, Fang Z, Ding H and Takahashi T 2010 *Phys. Rev. Lett.* **104** 137001

[24] Fujimori S, Saitoh Y, Okane T, Fujimori A, Yamagami H, Haga Y, Yamamoto E and Ōnuki Y 2007 *Nat. Phys.* **3** 618

[25] Jiang J, Li S, Zhang T, Sun Z, Chen F, Ye Z R, Xu M, Ge Q Q, Tan S Y, Niu X H, Xia M, Xie B P, Li Y F, Chen X H, Wen H H and Feng D L 2013 *Nat. Commun.* **4** 3010

[26] Opeil C P, Schulze R K, Manley M E, Lashley J C, Hults W L, Hanrahan R J Jr, Smith J L, Mihaila B, Blagoev K B, Albers R C and Littlewood P B 2006 *Phys. Rev. B* **73** 165109

[27] Opeil C P, Schulze R K, Volz H M, Lashley J C, Manley M E, Hults W L, Hanrahan R J Jr, Smith J L, Mihaila B, Blagoev K B, Albers R C and Littlewood P B 2007 *Phys. Rev. B* **75** 045120

[28] Liechtenstein A I, Anisimov V I and Zaanen J 1995 *Phys. Rev. B* **52** R5467

[29] Dudarev S L, Nguyen Manh D and Sutton A P 1997 *Philos. Mag. B* **75** 613

[30] Keast V J 2013 *Micron* **44** 93

[31] Maksimov E G, Mazin I I, Rashkeev S N and Uspenski Yu A 1988 *J. Phys. F: Met. Phys.* **18** 833

[32] Adachi S 2012 *The Handbook on Optical Constants of Metals* (World Scientific)

[33] Carroll J J and Melmed A J 1971 *J. Opt. Soc. Am.* **61** 470

[34] Wu J, Zhang Y, Chen Q, Wang Y, Feng W, Zhang Q, Yang X, Zhu X, Hao Q, Liu Q and Lai X 2024 *Appl. Surf. Sci.* **672** 160817

[35] Palstra T T M, Menovsky A A and Mydosh J A 1986 *Phys. Rev. B* **33** 6527

[36] Arajs S and Colvin R V 1964 *J. Less Common Met.* **7** 54

[37] Chen Q Y, Wen C H P, Yao Q, Huang K, Ding Z F, Shu L, Niu X H, Zhang Y, Lai X C, Huang Y B, Zhang G B, Kirchner S and Feng D L 2018 *Phys. Rev. B* **97** 075149

[38] Vyalikh D V, Danzenbächer S, Kucherenko Yu, Kummer K, Krellner C, Geibel C, Holder M G, Kim T K, Laubschat C, Shi M, Patthey L, Follath R and Molodtsov S L 2010 *Phys. Rev. Lett.* **105** 237601

[39] Ernst S, Kirchner S, Krellner C, Geibel C, Zwicknagl G, Steglich F and Wirth S 2011 *Nature* **474** 362

[40] Yuan X 2022 *Spin-Orbit Coupling in Strongly Correlated Systems* (Temple University)

[41] Santini P, Lémanski R and Erdős P 1999 *Adv. Phys.* **48** 537

[42] Yeh J J and Lindau I 1985 *At. Data Nucl. Data Tables* **32** 1

[43] Aynajian P, da Silva Neto E H, Parker C V, Huang Y, Pasupathy A, Mydosh J and Yazdani A 2010 *Proc. Natl. Acad. Sci. USA* **107** 10383

[44] Zhang Y, Lu H, Zhu X, Tan S, Feng W, Liu Q, Zhang W, Chen Q, Liu Y, Luo X, Xie D, Luo L, Zhang Z and Lai X 2018 *Sci. Adv.* **4** eaao6791

[45] Yang X, Wu J, Jiang Y, Liu Q, Chen Q, Zhang Q, Zhang Y, Fan X, Zhu X, Tan S, Hao Q, Feng W and Lai X 2025 *Appl. Surf. Sci.* **697** 163030

[46] Xu N, Matt C E, Pomjakushina E, Shi X, Dhaka R S, Plumb N C, Radović M, Biswas P K, Evtushinsky D, Zabolotnyy V, Dil J H, Conder K, Mesot J, Ding H and Shi M 2014 *Phys. Rev. B* **90** 085148

[47] Denlinger J D, Allen J W, Kang J S, Sun K, Kim J W, Shim J H, Min B I, Kim D J and Fisk Z 2013 arXiv:1312.6637 [cond-mat.str-el]